Impairment of bone remodeling in *LIGHT/TNFSF14*-deficient mice

Giacomina Brunetti (1), Maria Felicia Faienza (2), Graziana Colaianni (3), Isabella Gigante (1), Angela Oranger (1), Paolo Pignataro (1), Giuseppe Ingravallo (4), Adriana Di Benedetto (5), Sara Bortolotti (1), Mariasevera Di Comite (1), Giuseppina Storlino (1), Luciana Lippo (1), Lindsay Ward-Kavanagh (6), Giorgio Mori (5), Janne E. Reseland (7), Giovanni Passeri (8), Ernestina Schipani (9), Koji Tamada (10), Carl F. Ware (6), Silvia Colucci* (1), Maria Grano *(3).

(1) Department of Basic and Medical Sciences, Neurosciences and Sense Organs, section of Human Anatomy and Histology, University of Bari, Bari, Italy; (2) Department of Biomedical Science and Human Oncology, Paediatric Unit, University of Bari, Bari, Italy; (3) Department of Emergency and Organ Transplantation, Section of Human Anatomy and Histology, University of Bari, Bari, Italy; (4) Department of Emergency and Organ Transplantation, Pathology Section, University of Bari, Bari, Italy; (5) Department of Clinical and Experimental Medicine, University of Foggia, Foggia, Italy; (6) Infectious and Inflammatory Disease Center, Sanford Burnham Prebys Medical Discovery Institute, La Jolla, California, USA; (7) Department of Biomaterials, Institute for Clinical Dentistry, University of Oslo, Blindern, Oslo, Norway; (8) Department of Medicine and Surgery, University of Parma, Parma, Italy; (9) Departments of Medicine and Orthopaedic Surgery, University of Michigan, Ann Arbor, MI, USA; (10) Department of Oncology, Johns Hopkins University School of Medicine, Baltimore, Maryland, USA.
*These authors contributed equally.

Disclosures: All authors state that they have no conflicts of interest.

Corresponding Author:
Giacomina Brunetti, PhD
Department of Basic and Medical Sciences, Neurosciences and Sense Organs, section of Human
Anatomy and Histology, University of Bari,
Piazza Giulio Cesare, 11, 70124 Bari, Italy;
e-mail: giacomina.brunetti@uniba.it
Phone: +39 0805478306; Fax: +39 0805478361

ABSTRACT

Multiple cytokines produced by immune cells induce remodeling and aid in maintaining bone homeostasis through differentiation of bone forming osteoblasts and bone resorbing osteoclasts. Here, we investigate bone remodeling controlled by the TNF superfamily cytokine LIGHT. *LIGHT*-deficient mice (*Tnfsf14$^{-/-}$*) exhibit spine deformity, and reduced femoral cancellous bone mass associated with an increase in the osteoclast number and a slight decrease of osteoblasts compared to WT mice. The effect of LIGHT in bone cells can be direct or indirect, mediated by both the low expression of the anti-osteoclastogenic osteoprotegerin (OPG) in B and T cells, and reduced levels of the pro-osteoblastogenic *Wnt10b* in CD8$^+$ T cells in *Tnfsf14$^{-/-}$*mice. LIGHT stimulation increases OPG levels in B, CD8$^+$ T, and osteoblastic cells, as well as Wnt10b expression in CD8$^+$ T cells. The high bone mass in *Light* and T and B cell deficient mice (*Rag$^-$/Tnfsf14$^-$*) supports the cooperative role of the immune system in bone homeostasis. These results implicate LIGHT as a potential target in bone disease.

INTRODUCTION

Interactions between the immune system and bone cells are becoming increasingly important as continuous advances highlight new mechanisms and therapeutic targets for bone diseases (1). Indeed, several regulatory cytokines produced by immune cells can induce bone remodeling (2,3). Bone remodeling depends on the active balance of bone resorption and formation, which are mediated by osteoclasts (OCs) and osteoblasts (OBs) respectively (4,5). Shifting the balance in favor of OCs leads to diseases characterized by low bone mass, including osteoporosis. OCs originate from bone marrow-derived monocyte/macrophage lineage cells (BMMs), and their differentiation is positively and negatively modulated by the Tumor Necrosis Factor (TNF) superfamily members Receptor activator of NF-κB ligand (RANKL) and osteoprotegerin (OPG) respectively (3,6). OPG is primarily produced by bone marrow stromal cells, additionally IgM$^+$ B cells in bone marrow accounting for about 40% of the total OPG produced under basal conditions, although CD8$^+$ T cells also secrete a significant amount of OPG (7).

Another molecule with a key role in immune functions is LIGHT (homologous to *L*ymphotoxins exhibiting *I*nducible expression and competing with herpes simplex virus *G*lycoprotein D for herpes virus entry mediator [*H*VEM], a receptor expressed by *T* lymphocytes). LIGHT is a member of TNF superfamily (*TNFSF14*) and a key component of the TNF-lymphotoxin network (8-11). LIGHT is expressed in immune cells such as activated T cells, natural killer cells, monocytes, granulocytes, and immature dendritic cells (12-14).

LIGHT engages two membrane-bound signaling receptors, Herpes virus entry mediator (HVEM, TNFRSF14) and lymphotoxin-beta receptor (LTβR). HVEM is widely expressed in the hematopoietic lineage, as well as endothelial and epithelial cells (15-16). Through its interaction with HVEM, LIGHT acts as a potent T-cell co-stimulatory molecule (17-20) by counter-regulating the HVEM-BTLA (B- and T-lymphocyte attenuator) inhibitory checkpoint (8). LTβR is expressed on stromal cells and myeloid cell lineages where it controls lymphoid tissue development and homeostasis to contribute to the creation of an effective host defense system (9). Moreover, LIGHT

has been implicated in osteolytic rheumatoid arthritis and multiple myeloma (21-23) although conflicting results have been reported about the role of LIGHT in OC formation (21-24). While Hishida et al. reported no OC differentiation from peripheral blood CD14$^+$ monocytes treated with LIGHT (21), our previous work agreed with the pro-osteoclastogenic effects of LIGHT demonstrated by Edwards et al. and Hemingway et al. (22,24). However, all authors concordantly reported that LIGHT and RANKL synergistically stimulated OC formation (21-24). Furthermore, we found that LIGHT produced by immune cells inhibited osteoblastogenesis (23).

Given the results implicating LIGHT as a bone remodeling factor (23), we hypothesized that LIGHT deficiency could impair bone homeostasis. To demonstrate this hypothesis we conducted a detailed analysis of bone structure in *Tnfsf14$^{-/-}$* mice. We report that LIGHT contributes to the maintenance of skeletal physiology as revealed by the phenotype of cancellous bone loss. Importantly, LIGHT's effect on bone also involves T and B cells. Therefore, our findings indicate that LIGHT contributes to communication between the immune and skeletal systems.

METHODS

Mice. C57bl/6 mice deficient in *LIGHT* were obtained as previously described (25) and were backcrossed n=10. *Rag⁻/Tnsf14⁻* double knock-out (DKO) mice were generated by crossing a *Rag⁻/⁻* homozygous mouse with a *Tnfsf14⁻/⁻* homozygous mouse. Subsequent generations of heterozygotes were bred together to produce a line with homozygous knockouts of both the *Rag* and *Tnfsf14* genes. *Tnfsf14* heterozigous, *Rag⁻/⁻* and *Rag⁻/Tnsf14⁻* mice were kindly provided by prof. Carl F. Ware. Animals were housed four to five per cage at 23°C on a light/dark cycle and were fed a standard rodent chow.

At the end of the experimental procedure mice were euthanized and their tissues were surgically excised. Left femurs were subjected to bone marrow flushing. Vertebrae and right femurs were fixed with 4% (vol/vol) paraformaldehyde for 18 hours at 4°C and processed for histological analysis. This animal interventional study is in accordance with the European Law Implementation of Directive 2010/63/EU and all experimental protocols were reviewed and approved by the Veterinary Department of the Italian Ministry of Health.

Contact radiography. Mice were X-rayed by using contact radiography (Vista Scan Combi Durr Dental AG, Bietigheim-Bissingen). Scans were obtained by using a setting of 60 kV, 8 mA and 2.5 sec exposure time. The developed X-rays were scanned into a personal computer for image analysis. For spinal deformity evaluations, a first line was drawn between the caudal margin of the last cervical vertebra to the caudal margin of the sixth lumbar vertebra this line was divided by a second line perpendicular to this from the dorsal edge of the vertebra at the point of greatest curvature. The length of this second line was ratioed against those of the first line to account for potential differences in overall animal size, the resultant measure was used as measurement of spine deformity.

Microcomputed tomography. MicroCT scanning was performed to measure morphological indices of metaphyseal regions of right femurs. Bone samples were rotated around their long axes (0.4° as rotation step) and images were acquired using Bruker Skyscan 1172

(Kontich, Belgium) with the following parameters: voxel size = 6 μm^3; peak tube potential = 59kV; X-ray intensity = 167 μA; ring artefact correction = 10; beam hardening correction = 60%. Raw images were reconstructed by the SkyScan reconstruction software (NRecon) to 3-dimensional cross-sectional image data sets using a 3-dimensional cone beam algorithm. Structural indices were calculated on reconstructed images using the Skyscan CT Analyzer (CTAn) software (Bruker). Cortical and cancellous bone were separated using a custom processing algorithm in CTAn, based on the different thicknesses of the structures. Cortical bone was analysed by a region of 400 slices, starting 9 mm distal to the metaphysis. Cortical parameters included cortical thickness (Ct.Th), total cross-sectional area (Tt.Area), cortical bone perimeter (Ct.Pm) and marrow cross-sectional area (Marrow Area). Cancellous bone was analysed in the proximal metaphysis region starting just distal to the metaphysis and continued distally for 200 slices. Trabecular parameters included bone volume/total volume (BV/TV), number (Tb.N), thickness (Tb.Th), and separation (Tb.Sp) dimension (26).

Histological analysis of bone. Alizarin Red/Alcian Blue staining of new born skeleton was performed following protocols described by McLeod (27). Spines were decalcified, paraffin-embedded, cut into 5 μm slices and subjected to hematoxylin-eosin staining.

Lumbar vertebrae were embedded with Methylmethacrylate (MMA) after dehydration and the plastic sections were cut by a standard microtome (RM-2155 Leica, Heidelberg, Germany) into 7 μm for von Kossa staining and 5 μm for Tartrate-resistant acid phosphatase (TRAP). The sections were stained by the von Kossa silver impregnation with van Gieson counterstained method to determine cancellous BV/TV%, trabecular number (Tb.N, 1/mm) trabecular thickness (Tb.Th, mm) and trabecular separation (Tb.Sp, mm). For the analysis of OCs (OC number per bone perimeter, N.Oc/B.Pm), bone sections were incubated in TRAP staining solution and then counterstained with methyl green, whereas for OB analysis (OB number per bone perimeter, N.Ob/B.Pm) bone section were stained with toluidine blu. Microphotograph were captured under a microscope (Leica) using a 40x objective lens and analyzed by using Image-J software. For dynamic bone formation indices,

mice were injected with calcein (10 mg/kg body weight) and xylenol orange (90 mg/kg body weight), 10 and 2 days before sample collection (3 month mice), respectively. Unstained MMA-embedded cranial and femoral sections were analyzed to quantify the mineral apposition rate (MAR), bone formation rate (BFR) and mineralizing surface per bone surface (MS/BS).

Cell Cultures. Bone marrow (BM) was flushed from mouse femurs and tibia and cultured in α-MEM (Life Technologies) supplemented with 10% (vol/vol) FBS (Gibco, Life Technologies, Milan, Italy) and 1% penicillin/streptomycin (Life Technologies).

For OC differentiation, bone marrow cells were cultured with α-Minimal Essential Medium (α-MEM)/10% FBS, supplemented with 20 ng/mL of mouse macrophage colony-stimulating factor (MCSF; R&D system) and 30 ng/ml of mouse receptor activator of nuclear factor kappa-B ligand (RANKL; R&D system). At day 4, mature OCs were subjected to RNA extraction or were fixed and stained for TRAP. TRAP+ cells with more than three nuclei were counted as OCs. For the evaluation of OC activity, bone marrow cells were seeded on hydroxyapatite-coated coverslips. For some experiments mouse macrophages were cultured in the presence of MCSF and agonist antibody aHVEM (clone HM3.30, kindly provided by Prof Tamada K) or agonist antibody aLTβR (clone 4H8, kindly provided by Prof. Ware C) with or without RANKL and OC formation assessed. For osteogenic differentiation, bone marrow cells were cultured with α-MEM/10% FBS, supplemented with 50 μg/mL ascorbic acid and 10^{-2}M β-glycerophosphate. At day 10, cells were fixed in 3.7% (vol/vol) formaldehyde for 5 minutes and subjected to alkaline phosphatase (ALP) staining. Whereas to evaluate colony forming unit of OB (CFU-OB) formation at day 20, cells were fixed and von Kossa stained. Image J software was used to calculate area of ALP+ colony forming unit (CFU-F). For some experiments MC3T3 osteoblastic cells (Sigma Aldrich, Milan, Italy) cells were cultured in osteogenic medium in the presence of different concentration of agonist aLTβR (100 ng/ml), and ALP staining assayed.

Osteoblasts (5 digestion) and osteocytes (9 digestion) were isolated from the long bones of 6 month WT and *Tnsf14*⁻ mice as reported in literature (28), and subjected to mRNA extraction.

MC3T3 were seeded at $15000/cm^2$ and cultured in osteogenic medium with α-MEM/10% FBS, supplemented with 50 µg/mL ascorbic acid and 10^{-2} M β-glycerophosphate and treated for 2 or 10 days with or without 100 ng/ml agonist aLTβR. At the end of culture period, RNA extraction was performed to evaluate osteoblastic marker, RANKL and OPG expression. Furthermore, in media the levels of OPG and RANKL were assayed by mouse-specific ELISAs (R&D Systems).

Mesenchymal cells were isolated from WT mice, were seeded at $20000/cm^2$ and cultured in osteogenic medium with α-MEM/10% FBS, supplemented with 50 µg/mL ascorbic acid and 10^{-2} M β-glycerophosphate and treated for 2 or 10 days with or without 100 ng/ml agonist aLTβR. At the end of culture period, RNA extraction was performed to evaluate osteoblastic marker expression.

B- and T-cell isolation and OPG ELISA. The flushed BM was gently resuspended in red-cell lysis buffer followed by 2 washes with PBS. $CD4^+$ T and $CD8^+$ T cells were isolated from the flushed BM or the buffy coat from peripheral blood samples using CD4 and CD8 coated beads (Miltenyi Biotec GmbH, Bergisch Gladbach, Germany), respectively, according to the manufacturer's instruction.

B-lineage cells were purified from BM at different stages of differentiation based on the expression of specific makers. IgD^+ mature B cells were isolated using PE-IgD antibody and anti-PE-coupled immunomagnetic beads (Miltenyi Biotec). IgM^+ (immature) B cells were isolated using IgM-conjugated immunomagnetic beads following IgD depletion. The IgM antibody used is nonactivating. B-cell precursor cells (pre-proB, proB, large preB, and small preB) were purified using B220-coated immunomagnetic beads following IgM depletion. Plasma cells were isolated by CD138-conjugated immunomagnetic beads following B220 depletion using a $CD138^+$ Plasma Cell Isolation Kit (Miltenyi Biotec). Immunomagnetic bead isolation led to populations that were 96% pure, while depletion was 98% efficient as assessed by flow cytometry using BD Accuri™ C6 flow cytometer (Becton Dickinson, Mountain View, CA, USA). Conditioned media were generated by plating 1×10^7 purified B-lineage cells into 48-well plates in 1 mL per well of RPMI 1640

supplemented with 10% FBS and antibiotics. After 48 hours media were collected for analysis of OPG by mouse-specific ELISAs (R&D Systems).

Real Time-PCR. Total RNA was extracted using spin columns (RNeasy, Qiagen, Hilden, Germany) according to the manufacturer's instructions and reverse transcribed using iScript Reverse Transcription Supermix (Bio-Rad). The resulting cDNA (20 ng) was subjected to quantitative PCR (qPCR) using the SsoFast EvaGreen Supermix (Bio-Rad, Hercules, CA) on an iCycler iQ5 Cromo4 (Bio-Rad). Each transcript was assayed in triplicate and cDNA was normalized to β-Actin. The following primer pairs were used:

Ltβr: S:5′- CTAGGTCTCAGGCTTGCTCAGG-3′ AS: 5′-GCTCTACTCACCAGGACTCACAG-3′

Alp S:5′- AAACCCAGACACAAGCATTCC-3′ AS: 5′-TCCACCAGCAAGAAGAAGCC-3′

Collagen Type I (Cola1): S5′- GGCTCCTGCTCCTCTTAG-3′ AS: 5′-ACAGTCCAGTTCTTCATTGC- 3′;

Dentin matrix acidic phosphoprotein 1 (Dmp1): S5'-AGAGCAGGAGCCAGGAGAGC-3' AS: 5'-CCGATGGGTTTGTTGTGGTAAGC-3'

Osteocalcin (Ocn): S5'-CGCTCTGTCTCTCTGACCTCAC-3' AS: 5'-ACCTTATTGCCCTCCTGCTTGG-3';

Osterix (Osx): S 5'-AGTTCACCTGCCTGCCTGCTCTGTTC-3' AS: 5'-GCGGCTGATTGGCTTCTTCTTC -3';

Runx2: S 5'-CGTCAGCATCCTATCAGTTC-3' AS: 5'-CCGTCAGCGTCAACACCATC-3';

Osteopontin (Opn): S 5'-ATCTCAGAAGCAGCCTCTCC-3' AS: 5'ATCCTCATCATCGTCGTCC-3';

Atf4: S 5'-GCCTGACTCTGCTGCTTACATTAC-3' AS: 5'-CACGGGAACCACCTGGAGAAG-3';

Trap: S 5′- GCAGCAGCCAAGGAGGACTAC-3′ AS:5′-AGCACATAGCCCACACCGTTC-3′

Cathepsin K (Ctsk): S: 5′-GGGTGTTCAAGTTTCTGCTGCTAC-3′ AS 5′-

ACTGCTTCTGGTGAGTCTTCTTCC-3′

Oscar: S:5'-GCGTAGGCGTGGCAACCC-3' AS:5'-CAGAAGGCGTGGTAATAGCAAC-3'

Integrin β3 (Intβ3) S:5'-GTGAGTGCTCTGAGGAGGATTACC-3' AS:5'-AS

TGCCGAAGTCGCTGCTATGG-3';

Cfms S:5'-ATGCCCGCCTGCCTGTAAAG-3' AS:5'CCGTAGGACCACACATCACTCTG-3'

Aptase6   S:5'-AAAGCCAGCCTCCTAACTCAGC-3'; AS:5'-

AGTTGCCATAGTCCGTGGTCTG-3';

Dcstamp S: 5'-CTGCTGTATCGGCTCATCTCCTC-3'; AS:5'-

ACTCCTTGGGTTCCTTGCTTCTC;

Rank S: 5'-TCGTTCTGCTCCTCTTCATCTCTG-3'; AS:5'-

GGTGCTGATGACTGCCAAGATTG-3';

Rankl S: 5′- CAGGAGGATGAAACAAGCC-3′ AS: 5′-GCAGCATTGATGGTGAGG-3′

Opg S 5′- GACCACTCTTATACGGACAG-3′ AS 5′-CTCACACTCACACACTCG- 3′

β-catenin S: 5′-AAAACCATTCCCACCCTAC-3′ AS 5′-AGCTGGCCTGGTTTGATAC- 3′

β-actin S: 5′- CTCCTAGCACCATGAAGATCAAGAT-3′ AS: 5′-

CTGCGCAAGTTAGGTTTTGTCAAAG-3′.

Quantitative measures were obtained as previously reported (29).

Statistical analysis. Statistical analyses were performed by ANOVA or Student's t-test with the Statistical Package for the Social Sciences (spssx/pc) software (SPSS, Chicago, IL, USA). The results were reported as Mean ± Standard deviation (SD) and considered statistically significant for $p < 0.05$.

RESULTS

Tnfsf14^{-/-} mice have spine deformity and reduced femur cancellous bone mass. We have previously reported that LIGHT affects bone remodelling by exerting both a pro-osteoclastogenic

and an anti-osteoblastogenic effect (23). These findings prompted us to study the bone phenotype of *Tnfsf14*^{-/-} mice in comparison with age- and sex-matched wild-type (WT) mice. We found that approximately 40% of newborn *Tnfsf14*^{-/-} mice exhibit a spinal deformity in the curvature of the spine at thoracic vertebrae (Fig. 1A) as detected by alizarin red/alcian blue staining of bone and cartilage tissues. This deformity was confirmed by x-ray (Fig. 1B) and it was persistent and did not change over time in *Tnfsf14*^{-/-} mice compared to WT (Fig. 1C). Consistently, haematoxylin-eosin staining of spine sagittal sections from 3 month mice showed that the end plates of *Tnfsf14*^{-/-} mice had a disorganization of the chondrocyte columns at thoracic vertebrae. In particular, *Tnfsf14*^{-/-} mice showed a significant reduction column height and number of cells for hypertrophic zone (HZ) and proliferative zone (PZ), respectively (Fig. 1D). The alteration of HZ is also evident in 12 month mice *Tnfsf14*^{-/-} mice (Fig. 1D). Histomorphometric analysis performed on von Kossa-stained lumbar vertebrae of 3- and 6-month *Tnfsf14*^{-/-} mice did not show any alterations between the two groups of animals (Fig. 1E).

We evaluated the distal femoral cancellous and cortical bone compartments of 1, 3, 6 and 12-month WT and *Tnfsf14*^{-/-} mice by microCT. Surprisingly, femur reconstructions showed severely reduced cancellous bone structure in *Tnfsf14*^{-/-} mice at all the evaluated ages of mice (Fig. 2). Indeed, we demonstrated a significant decrease in trabecular bone volume per tissue volume (BV/TV) in *Tnfsf14*^{-/-} mice, resulting from a significant decrease in trabecular thickness (Tb. Th.), and number (Tb. N.) as well as an increase in trabecular spacing (Tb. Sp.) (Fig. 2). Bone architecture denoted by the structure model index (SMI) was not significantly altered (not shown), nor was the cortical compartment (Table 1).

By timed injections of xylenol orange and calcein, we analyzed dynamic histomorphometry of cranial bone as well as femoral cortical and cancellous bone showing a significant decrease in bone formation parameters. We demonstrated the reduction of BFR and bone surface/mineralised surface ratio (MS/BS) in Tnfsf14-/- mice with respect to WT controls (Fig. 3A, B and C). Only in

femoral cancellous bone mineral apposition rate (MAR) significantly decrease in Tnfsf14-/- mice with respect to WT controls (Fig. 3C).

In addition, a slight but significant decrease in OB cell numbers, as measured by counting the epitheloid cells on the bone perimeter (Fig. 3D), as well as a strong increase in tartrate-resistant acid phosphatase (TRAP)-stained OC number per bone perimeter were observed in *Tnfsf14*^{-/-} mice (Fig. 3E).

Tnfsf14^{-/-} **mice display increased osteoclastogenesis in** *ex vivo* **cultures.** To investigate whether the increase in OC number in *Tnfsf14*^{-/-} mice correlated with an enhancement of OC formation and activity, we performed *ex vivo* bone marrow cell cultures from 1-, 3-, 6-, 12-month old *Tnfsf14*^{-/-} mice in the presence of RANKL, a molecule essential for generating bone resorbing cells in culture. We observed an increase in OC formation (Fig. 4A), and a significant increase in their bone resorbing activity (Fig. 4B), in cultures derived from 1-, 3-, 6-, 12-month old *Tnfsf14*^{-/-} mice compared with WT mice as quantified in graphs (Fig. 4A-B). Likewise, by analysing the levels of different osteoclastic master genes, we demonstrated greater expression of the genes encoding the receptors for MCSF (*Cfms*) and RANKL (*Rank*), the Integrin β3 (*Int β3*), and the two marker enzymes cathepsin K (*Ctsk*) and *Trap* in mature OC cultures derived from *Tnfsf14*^{-/-} mice compared with WT mice of 6-month WT and *Tnfsf14*^{-/-} mice (Fig. 4C). The same trend was observed in OC cultures derived from 1-, 3-, and 12 month mice (data not shown). These findings suggest that under physiological conditions LIGHT can be considered an anti-resorptive cytokine, as the loss of LIGHT signalling enhanced OC formation and bone resorption.

In contrast, *ex vivo* OB differentiation in bone marrow stromal cell cultures from 1-, 3-, 6-, 12-month *Tnfsf14*^{-/-} mice supplemented with ascorbic acid and β-glycerophosphate did not demonstrate any significant change in the percentage of ALP-positive colony forming-fibroblastoid (CFU-F) colonies (Fig. 4D), a parameter of early stage OB differentiation. Similarly, we did not observe any differences in the development of von Kossa-positive mineralizing nodules (CFU-

13

OBs), a marker of osteoblastic bone forming activity in cultures derived from *Tnfsf14*^{-/-} mice (Fig. 4E).

***In vitro* LIGHT effect on bone cell differentiation.** The results from the *ex vivo* experiments prompted us to evaluate the effect of LIGHT on bone cell differentiation *in vitro* by treating cultures with agonist antibodies to HVEM (aHVEM) or LTβR (aLTβR) that mimicked only LIGHT activity. We first assessed osteoclastogenesis in cultures of WT macrophages previously demonstrated to express both LIGHT receptors. We found that macrophages did not differentiate into OCs in the presence of agonist antibodies utilized alone. However, combining aHVEM or aLTβR with RANKL produced an increased OC formation compared with RANKL alone (Fig. 5A). A control IgG did not affect osteoclastogenesis (data not shown). Since BM precursor cultures include hematopoietic cells that could affect osteoblastogenesis, we tested the effect of aLTβR on osteoblastogenesis in the MC3T3 osteoblastic cell line and murine mesenchymal cells as these cells expressed only *Ltβr* during the differentiation process (Fig 5B-5C). MC3T3 cells and mesenchymal cells were cultured with 100ng/ml aLTβR or a control IgG in the presence of ascorbic acid and β-glycerophosphate, and the expression of OB markers was evaluated at days 2 and 10. We found that exposure to 100ng/ml aLTβR modified expression of several genes in MC3T3 and mesenchymal cells at either time point of the differentiation (Fig. 5B), otherwise low aLTβR concentration did not affect osteoblastogenesis (data not shown). Specifically, in MC3T3 after 2 days of differentiation aLTβR treatment significantly decreased the expression of *Alp* and *Osx*, whereas at 10 days the expression of additional genes, such as *Dmp1*, *Opn* and *Cola1* was also modulated. Differently, in mesenchymal cells after 2 days of differentiation aLTβR treatment significantly decreased only the expression of *Osx*, while at 10 days also the expression of numerous genes resulted modulated, as *Runx2*, *Dmp1*, *Atf4*, *Opn* and *Cola1*. Conversely, the control IgG did not affect the expression of such factors (data not shown).

14

LIGHT involvement in the regulation of RANKL and OPG in the osteoblastic lineage.
The increase of OCs in *Tnfsf14*^{-/-} together with the lack of a LIGHT direct pro-osteoclastogenic effect without RANKL let us to hypothesized that LIGHT deficiency could also indirectly affects osteoclastogenesis. Furthermore, the spine deformity and reduced cancellous bone mass are features also observed in *Opg*-deficient mice (30), thus we investigated *Opg* levels in cells of the osteoblastic lineage and immune cells, which are both known to secrete OPG (7,30). Firstly, to determine if OBs could respond to LIGHT stimulation by producing OPG and/or RANKL, we treated MC3T3 cultured in osteogenic medium with 100 ng/ml aLTβR for 2 and 10 days, resulting in a strong increase of OPG and a reduction of RANKL at protein levels as well as their respective transcripts, thus resulting in a significant reduction of RANKL/OPG ratio with an anti-osteoclastogenic effect (Fig. 6A). In the same cultures an irrelevant IgG did not affect RANKL and OPG levels (data not shown). These results prompted us to evaluate *Opg* and *Rankl* levels in OBs and osteocytes freshly isolated following multiple digestions of cortical bone of WT and *Tnfsf14*^{-/-} mice (Fig. 6B). Although there was a trend towards the increase of *Opg* and a reduction of *Rankl*/*Opg* ratio in cells isolated from *Tnfsf14*^{-/-} mice compared to WT mice, it did not reach a statistical significance. Consistently, we did not find significant differences in the expression of *Opg* and *Rankl*, and thus for *Rankl*/*Opg* ratio in CFU-F and CFU-OB mRNA extracts derived from WT and *Tnfsf14*^{-/-} mice (data not shown). These findings lead us to hypothesize an immune-mediated mechanism of bone homeostasis by LIGHT.

Opg and Wnt10b mediate the effect of LIGHT on bone cell differentiation. To explore the role of immune cells we firstly investigated *Opg* and *Rankl* levels in total bone marrow lysates and secondly in B and T cells. *Opg* mRNA levels in total bone marrow cell lysates were substantially decreased in *Tnfsf14*^{-/-} mice, an observation that was already evident at 1 month of age and persisted at 3, 6 and 12 months (Fig. 7A). In contrast, *Rankl* levels were unchanged in total bone marrow cell lysates (Fig. 7B). Measurement of OPG protein in conditioned medium from 1 ×

10^7 total bone marrow cells also demonstrated reduced levels of OPG production by *Tnfsf14^(-/-)* mouse cells compared to WT (Fig. 7D) as well as unmoved RANKL levels (Fig 7E). These data indicated that the RANKL/OPG ratio skews toward RANKL in *Tnfsf14^(-/-)* mice both in total bone marrow lysates and conditioned media (Fig. 7C, 7F).

As we did not find significant differences in the expression of *Opg* and *Rankl* in osteoblastic cells derived from WT and *Tnfsf14^(-/-)* mice and OPG in the BM is primarily produced by B cells, with minor contributions from T cells (7,31), we analysed these cell populations to determine if their production of *Opg* was affected by LIGHT. In the same cells from WT and *Tnfsf14^(-/-)* mice the expression of *Rankl* was also evaluated, but we did not find statistical significant differences (data not shown). The reported data refers to 3 month old mice, but a similar trend was observed at 1, 6 and 12 months. T cells isolated from the bone marrow of *Tnfsf14^(-/-)* mice demonstrated a significant reduction of *Opg* mRNA levels with consequent increase of *Rankl/Opg* ratio in CD8+ T cells (Fig. 7G, 2.5 fold), whereas no differences were found for CD4+ T cells (Fig. 7H). We also investigated *Opg* production in B cell subsets separated by immunomagnetic panning. We found a 2-fold reduction of *Opg* mRNA levels in preB B cell precursors, immature B cells and mature B cells in *Tnfsf14^(-/-)* mice with respect to WT, whereas no difference was observed in plasma cells (Fig. 7I-L). Consistently, a significant increase of *Rankl/Opg* ratio in the mentioned B cell subpopulation, but not in plasma cells was found (Fig. 7I-L). OPG protein levels were also decreased in the media derived from cultures of CD8+ T cells or IgM+ B cell subpopulations from *Tnfsf14^(-/-)* mice (WT: 22.4 ± 3.4 vs *Tnfsf14^(-/-)*: 15.1 ± 2.3 pg/ml, p<0.01; WT: 25.7 ± 4.3 vs *Tnfsf14^(-/-)*: 16.2 ± 3.9 pg/ml; p<0.01, respectively). These findings were not associated with variation in the percentage of the different T and B cell subpopulations in the bone marrow of WT and *Tnfsf14^(-/-)* mice (data not shown). Interestingly, *Opg* expression was drastically reduced in mRNA lysates of peripheral blood samples (Fig. 7M), with a significant decrease observed in both circulating CD8+ T cells and mature B cells from *Tnfsf14^(-/-)* mice compared to WT mice (Fig. 7N-O). In the same cell populations *Rankl* expression did not result significant modulated (data not shown), however the *Rankl/Opg* ratio is

significant higher in *Tnfsf14*$^{-/-}$ mice compared to WT mice (Fig. 7N-O). However, neither total mRNA spleen extracts (Fig. 7P) nor sera protein levels from *Tnfsf14*$^{-/-}$ and WT mice exhibited significant differences in OPG and RANKL levels, as well as RANKL/OPG ratio (Fig. 7Q, 7K and 7S, respectively).

While defects in LIGHT decrease OPG production, aHVEM treatment of BM CD8$^+$ T cells and IgM$^+$ B cells from WT mice consistently induced a dose-dependent increase of OPG release (Fig. 7T).

To identify the possible mediator of LIGHT's effect on OB differentiation we investigated the expression of *Wnt10b*. This pro-osteoblastogenic factor is known to be produced by CD8$^+$ T-cells (32), a T cell subset that exhibits impaired activity in *Tnfsf14*$^{-/-}$ mice (33,34). We observed a significant decrease of this transcript in mRNA extracted from the CD8$^+$ T cells from *Tnfsf14*$^{-/-}$ mice at 1, 3, 6 and 12 months of age (Fig. 7U). Consistently, we also demonstrated that a 24 hour treatment with 100 ng/ml aHVEM induced a 2.8-fold increase of *Wnt10b* transcript expression in CD8$^+$ T cells from WT mice (Fig. 7V). As the final effector of Wnt10b is *β-catenin* (32) we evaluated its expression in OBs from our mice. We found a slightly significant reduction of *β-catenin* expression in OBs from *Tnfsf14*$^{-/-}$ mice compared to WT once (Fig. 7W).

***Rag*$^-$/*Tnfsf14*$^-$ DKO mice showed increased bone mass compared to *Tnfsf14*$^{-/-}$ mice.** To further explore the B and T cell-mediated effects of LIGHT on bone, we performed microCT to evaluate the femoral microstructure of *Tnfsf14*$^{-/-}$ mice bred onto *Rag*-deficient mice, a strain that does not develop mature T or B cells (35). Consistently, femur reconstructions from DKO mice showed a significant increase of cancellous bone structure with respect to *Rag*$^{-/-}$ mice (Fig. 8A). Indeed, we demonstrated a significant 33 % increase in trabecular BV/TV in DKO mice resulting from a significant increase in Tb. Th. (13.1%), and Tb. N. (11.6%), as well as a 42% decrease in Tb. Sp. (Table 2a). The cortical compartment was not significantly affected despite trends toward increasing cortical thickness (Co. Th.) and decreasing bone marrow area in DKO (Fig. 8A, Table

17

2b). Consistently, DKO displayed a strong reduction of OC number (Fig. 8B) as well as a slight increase of OB number per bone perimeter (Fig. 8C). These results prompted us to evaluate *Opg* and *Rankl* expression in total bone marrow lysates from the same mice. DKO displayed a 20-fold increase in levels of *Opg* and a 3.5 increase of *Rankl* compared to *Rag*^{-/-} mice, with consequent reduced *Rankl/Opg* ratio in the former compared to the latter (Fig. 8D). Interestingly, DKO mice display increased level of *Rankl* and *Opg* compared to *Tnfsf14*^{-/-} mice, but the lowest levels of *Rankl/Opg* ratio compared to both *Rag*^{-/-} and *Tnfsf14*^{-/-} mice. These results suggested that LIGHT effect on basal bone remodelling is mainly mediated by T- and B-cells.

DISCUSSION

Our study defines a novel role for LIGHT in the maintenance of skeletal physiology as LIGHT deletion produces cancellous bone loss. LIGHT deficiency is accompanied by dramatically increased osteoclastic bone resorption, and slightly diminished osteoblastic bone formation. Importantly, LIGHT's effect on bone cells involves T and B cells. In fact, treatment of these immune cells with agonist aHVEM, mimicking LIGHT activity, significantly enhanced the levels of the osteoclastic inhibitor OPG, and enhances expression of the osteoblastic stimulator *Wnt10b* (Figure 9). We hypothesize, therefore, that LIGHT is fundamental to immune system-bone communication, and thus highlights a new mechanism regulating the crosstalk between these systems.

The loss of *LIGHT* not only alters femoral cancellous bone, but also spine as typified by lifelong deformity that develops in newborn mice. Interestingly, a genetic locus for adolescent idiopathic scoliosis is reported linked to chromosome 19p13.3, a region that includes the *Tnfsf14* gene (36), suggesting that deepening the study of *Tnfsf14* in humans could lead to new preventive and therapeutic strategies. The persistent spine deformity seems to be associated with a defect of thoracic vertebrae. In fact, histomorphometric analysis in lumbar vertebrae did not show differences between WT and *Tnfsf14*^{-/-}, this is not unexpected as thoracic and lumbar vertebrae have different

functions and have a different response to the mechanical loading. Furthermore, the different behavior of vertebrae and femora in *Tnfsf14$^{-/-}$* mice is not surprising since several studies reported that some cytokines can display site specific bone effects (37-38). Furthermore, we can speculate that the marrow immune cells, present in close proximity of bone surfaces, impaired the BFR in *Tnfsf14$^{-/-}$*cortical bone of the femora and cranium.

Consistent with our findings, spine deformity and bone loss in the cancellous compartment are also typical features of *Opg$^{-/-}$* mice (30). *Opg$^{-/-}$* mice also showed an alteration of the cortical compartment, a result of the complete OPG expression loss in all cells of the mouse, unlike our model showing "normal" levels of *Opg* in osteoblasts and osteocytes. LIGHT stimulation through aHVEM did increase OPG expression in CD8^{+} T and B cells, whereas osteoblastic cell signalling required aLTβR treatment. Furthermore, aLTβR treatment decreased *Rankl* expression in MC3T3 cells, thus further exerting an anti-osteoclastogenic effect and supporting the protecting role of LIGHT on bone. Interestingly, by *in vitro* experiments we showed that B and CD8^{+} T cells are more sensitive to LIGHT effect compared to MC3T3 which are sensitive to major concentration of the ligand compared to the immune cells. These findings could also explain the lack of *Opg* and *Rankl* alteration as wells as of *Rankl/Opg* ratio in OBs and osteocytes from *Tnfsf14$^{-/-}$* mice, as the low physiological concentration of LIGHT did not affect osteoblastic cells. Consistently, we did not find significant difference of the *Rankl/Opg* ratio in CFU-Fs and CFU-OBs from *Tnfsf14$^{-/-}$* mice. Moreover, since osteoblastic cells did not express LIGHT, B and T cells, the main source of the cytokine, are the primary targets resenting of *LIGHT* deficiency.

In basal conditions of bone modeling and remodeling, the RANKL/OPG ratio is the major mechanism of osteoclastogenesis regulation. Human polymorphisms in the *Opg* gene have been linked both to low bone mineral density (39) and augmented incidence of fracture (40). Our study highlighted the role of LIGHT *in vivo* through OPG regulation in immune cells, but not RANKL. These findings suggest that in *Tnfsf14$^{-/-}$* mice cancellous bone loss was driven by an unbalancing of the RANKL:OPG ratio in favour of RANKL that skewed bone towards OC differentiation.

Interestingly, in our experiments OPG levels and the RANKL/OPG ratio were significantly modulated only in immune cell lysates and culture media from *Tnfsf14*^{-/-} mice compared to WT, but not in the sera. These findings could be explained by our experiments demonstrating that only immune cells and not the osteoblastic cell lineage of the *Tnfsf14*^{-/-} mice showed reduced expression of *Opg*. Furthermore, we did not find significant differences of *Opg* expression in the spleen from WT and *Tnfsf14*^{-/-} mice probably because this organ produces the lowest levels of OPG respect to the bone marrow and the peripheral blood (7) and has a major number of plasma cells compared to the bone marrow (7).

The immune cell subsets that we found affected by LIGHT were CD8^{+} T cells and B cells. To demonstrate that the alteration of these cells is crucial to the bone phenotype induced by LIGHT we studied *Tnfsf14*^{-/-} mice crossed to *Rag*^{-/-} mice, a strain that lacks mature T and B cells (35). These mice displayed increased BV/TV%, Tb.Th, and a decrease of Tb.Sp in the cancellous compartment compared to *Rag*^{-/-} mice, together with a reduced number of OCs and an increased OB counts. Consistently, total bone marrow lysates from DKO mice displayed the highest levels of *Opg* and lowest *Rankl/Opg* ratio compared to *Tnfsf14*^{-/-} and *Rag*^{-/-} mice. Taking into account that OBs and osteocytes from *Tnfsf14*^{-/-} displayed a trend in increasing *Opg* levels compared to WT mice, it is possible that in DKO mice the cells of the osteoblastic lineage together with immature immune cells could produce the OPG necessary to rebuild the bone of *Rag*^{-/-} mice. However, the effect of other growth factors can not be excluded in the bone rescue of DKO mice. Thus, the lack of mature B and T cells and the simultaneous absence of LIGHT expression showed that LIGHT can affect bone through the modulation of OPG expression by cells of immune system.

Consistently, we showed that production of OPG by CD8^{+} T cell- and B cell increases in response to aHVEM, an antibody mimicking LIGHT, treatment. Physiologically, LIGHT serves as a co-stimulatory molecule for T cell activation, leading to enhanced proliferation and Th1-type cytokine production (17). Because LIGHT is expressed by activated T cells, and activated T cells

also secrete large amounts of RANKL (41) it is possible that the increase in OPG levels induced by LIGHT could be useful to counteract RANKL and protect bone during an immune response.

In accordance with the key role of B and T cells in our model, Li et al. found that femurs from B cell-deficient mice showed profoundly reduced cancellous bone and a low thinning of the cortical bone by microCT (7). Choi et al. also reported that activated CD8$^+$ T cells inhibited OC differentiation and activity induced by RANKL (31), while John et al. demonstrated that depletion of CD8$^+$ T cells from murine bone marrow cells increased osteoclastogenesis during co-culture of the marrow cells and a murine calvarial-derived cell line (42). This literature suggests that both activated and naive CD8$^+$ T cells inhibit osteoclastogenesis *in vitro*. Among the proposed mechanisms, it has been reported that activated CD8$^+$ T cells inhibit OC formation by functioning as a source of OPG. In our system, reduced *Opg* expression by CD8$^+$ T cells in *Tnfsf14$^{-/-}$* mice appears to be a part of the defective activation phenotype resulting from LIGHT deficiency, as this mouse strain has previously been demonstrated to develop a normal number of CD8$^+$ T cells (33,34).

Consistent with their low OPG production by T and B cells, *Tnfsf14$^{-/-}$* mice developed increased numbers of OCs both *in vivo* and in *ex vivo* cultures compared to WT mice. Furthermore, in the presence of agonist aLTβR or aHVEM antibodies that mimic LIGHT activity, *in vitro* macrophages failed to differentiate into OCs, whereas simultaneous exposure of murine macrophages to the each antibody and RANKL synergized to drive OC formation. This finding of synergistically promoting OC formation has been demonstrated by us and other authors using human monocytes, and has been linked to pathological bone resorption associated with rheumatoid arthritis and multiple myeloma (22,23). Thus, it is possible that if chronic inflammation persists, reaching high LIGHT level, the same molecule fails to protect bone and instead activates additional mechanisms responsible for bone lesion development. In fact, high concentration of aLTβR inhibited the expression of major markers of OB differentiation in MC3T3 and mesenchymal cells. These two different type of cells did not show a complete overlap in the modulation of major

21

osteoblastic markers following aLTβR treatment, probably because MC3T3 are a cell line derived from calvaria, whereas mesenchymal cells are primary cells isolated from the bone marrow.

Consistent with the CD8$^+$ T cell impairment in *Tnfsf14$^{-/-}$* mice (33,34) we found these T cells also exhibited reduced levels of the anabolic molecule Wnt10b. These differences could be the cause of the slight reduction in OB number, BFR, and MS/BS measurements. Consistently, freshly isolated OBs from *Tnfsf14$^{-/-}$* mice showed slightly reduced expression of β-catenin, that is fundamental for the activation of transcription factors involved in osteoblastogenesis (32).

A similar mechanism has been proposed for another co-stimulatory molecule, CD40L. *CD40L$^{-/-}$* mice showed reduced cancellous and cortical bone mass which was associated with reduced OPG levels compared to WT mice (7). It is important to specify that CD40L ligation represents an early event in T cell activation (< 24 h) and is of short duration (< 72 h), while LIGHT induction peaks at 48 h and expression lasts for 4 days (43). Thus, we can speculate that CD40L and LIGHT together or alternately contribute to protecting bone under basal conditions. Consistent with this hypothesis, *CD40L$^{-/-}$* mice showed reduced bone mass, and B cell-deficient mice were demonstrated to be more osteoporotic with reduced amounts of BM OPG (7).

Taken together, our data add another crucial mechanism to the biological evidence supporting the tight relationship between the immune system and the skeleton. This could further highlight how the immune system may trigger a skeletal anabolic response, thus protecting bone by limiting basal bone resorption *in vivo*. Whether these effects in mice recapitulate human physiology requires further study. In particular, high levels of LIGHT in humans have been associated with bone loss (22,23) suggesting that LIGHT can have both anabolic and catabolic effects on bone depending on its levels. Thus, the therapeutic potential of LIGHT agonists or antagonists will require further study.

REFERENCES

1. Ono T, Okamoto K, Nakashima T, et al. IL-17-producing γδ T cells enhance bone regeneration. Nat Commun. 2016; 7:10928

2. Mori G, D'Amelio P, Faccio R, Brunetti G. The Interplay between the bone and the immune system. Clin Dev Immunol. 2013;2013:720504.

3. Takayanagi H. Osteoimmunology: shared mechanisms and crosstalk between the immune and bone systems. Nat. Rev. Immunol. 2007; 7: 292–304.

4. Karsent G and Wagner EF. Reaching a genetic and molecular understanding of skeletal development. Dev. Cell. 2002; 2, 389–406.

5. Teitelbaum SL and Ross FP. Genetic regulation of osteoclast development and function. Nat Rev Genet. 2003; 4: 638–649.

6. Novack DV and Mbalaviele G. Osteoclasts-Key Players in Skeletal Health and Disease. Microbiol Spectr. 2016; 4(3).

7. Li Y, Toraldo G, Li A, et al. B cells and T cells are critical for the preservation of bone homeostasis and attainment of peak bone mass in vivo. Blood. 2007; 109(9):3839-48.

8. Šedý J, Bekiaris V, Ware CF. Tumor necrosis factor superfamily in innate immunity and inflammation. Cold Spring Harb Perspect Biol. 2014; 7(4):a016279.

9. Gommerman JL, Browning JL, Ware CF. The Lymphotoxin Network: orchestrating a type I interferon response to optimize adaptive immunity. Cytokine Growth Factor Rev. 2014; 25(2):139-45.

10. Steinberg MW, Cheung TC, Ware CF. The signaling networks of the herpesvirus entry mediator (TNFRSF14) in immune regulation. Immunol Rev. 2011; 244(1):169-87.

11. Ware CF, Sedý JR. TNF Superfamily Networks: bidirectional and interference pathways of the herpesvirus entry mediator (TNFSF14). Curr Opin Immunol. 2011; 23(5):627-31.

12. Mauri DN, Ebner R, Montgomery RI, et al. LIGHT, a new member of the TNF superfamily, and lymphotoxin α are ligands for herpesvirus entry mediator. Immunity. 1998; 8:21–30.

13. Tamada K, Shimozaki K, Chapoval AI, et al. LIGHT, a TNF-like molecule, costimulates T cell proliferation and is required for dendritic cell-mediated allogeneic T cell response. J Immunol. 2000; 164:4105–4110.

14. Holmes TD, Wilson EB, Black EV, et al. Licensed human natural killer cells aid dendritic cell maturation via TNFSF14/LIGHT. Proc Natl Acad Sci U S A. 2014: 111(52):E5688-96.

15. Harrop JA, Reddy M, Dede K, et al. Antibodies to TR2 (herpesvirus entry mediator), a new member of the TNF receptor superfamily, block T cell proliferation, expression of activation markers, and production of cytokines. J Immunol. 1998; 161:1786–1794.

16. Kwon BS, Tan KB, Ni J, et al. A newly identified member of the tumor necrosis factor receptor superfamily with a wide tissue distribution and involvement in lymphocyte activation. J Biol Chem. 1997; 272:14272–14276.

17. Tamada K, Shimozaki K, Chapoval AI, et al. Modulation of T-cell-mediated immunity in tumor and graft-versus-host disease models through the LIGHT co-stimulatory pathway. Nat Med. 2000; 6:283–289.

18. Wang J, Lo JC, Foster A, et al. The regulation of T cell homeostasis and autoimmunity by T cell-derived LIGHT. J Clin Invest. 2001; 108:1771–1780.

19. Harrop JA, McDonnell PC, Brigham-Burke M, et al. Herpesvirus entry mediator ligand (HVEM-L), a novel ligand for HVEM/TR2, stimulates proliferation of T cells and inhibits HT29 cell growth. J Biol Chem. 1998; 273:27548–27556.

20. Marsters SA, Ayres TM, Skubatch M,et al. Herpesvirus entry mediator, a member of the tumor necrosis factor receptor (TNFR) family, interacts with members of the TNFR-associated factor family and activates the transcription factors NF-kappaB and AP-1. J Biol Chem. 1997; 272:14029–14032.

21. Ishida S, Yamane S, Nakano S, et al. The interaction of monocytes with rheumatoid synovial cells is a key step in LIGHT-mediated inflammatory bone destruction. Immunology. 2009: 128:e315–e324.

22. Edwards JR, Sun SG, Locklin R, et al. LIGHT (TNFSF14), a novel mediator of bone resorption, is elevated in rheumatoid arthritis. Arthritis Rheum. 2006: 54:1451–1462.

23. Brunetti G, Rizzi R, Oranger A, et al. LIGHT/TNFSF14 increases osteoclastogenesis and decreases osteoblastogenesis in multiple myeloma-bone disease. Oncotarget. 2014; 5(24):12950-67.

24. Hemingway F, Kashima TG, Knowles HJ, et al. Investigation of osteoclastogenic signalling of the RANKL substitute LIGHT. Exp Mol Pathol. 2013; 94:380–385.

25. Scheu S, Alferink J, Pötzel T, Barchet W, Kalinke U, Pfeffer K. Targeted disruption of LIGHT causes defects in costimulatory T cell activation and reveals cooperation with lymphotoxin beta in mesenteric lymph node genesis. J Exp Med. 2002;195(12):1613-24.

26. Bouxsein ML, Boyd SK, Christiansen BA, Guldberg RE, Jepsen KJ Müller R. Guidelines for assessment of bone microstructure in rodents using micro–computed tomography. J Bone Miner Res. 2010;25: 1468-86.

27. McLeod MJ. Differential staining of cartilage and bone in whole mouse fetuses by Alcian Blue and Alizarin Red S. Teratology. 1980; 22(3):299–301.

28. Shah KM, Stern MM, Stern AR, Pathak JL, Bravenboer N, Bakker AD. Osteocyte isolation and culture methods. Bonekey Rep. 2016;5:838.

29. Colucci S, Brunetti G, Mori G, et al. Soluble decoy receptor 3 modulates the survival and formation of osteoclasts from multiple myeloma bone disease patients. Leukemia. 2009; 23(11):2139-46.

30. Bucay N, Sarosi I, Dunstan CR, et al. Osteoprotegerin-deficient mice develop early onset osteoporosis and arterial calcification. Genes Dev. 1998; 12(9):1260-8.

31. Choi Y, Woo KM, Ko SH, et al. Osteoclastogenesis is enhanced by activated B cells but suppressed by activated CD8(+) T cells. Eur J Immunol. 2001; 31(7):2179-88.

32. Terauchi M, Li JY, Bedi B, et al. T lymphocytes amplify the anabolic activity of parathyroid hormone through Wnt10b signaling. Cell Metab. 2009; 10(3):229-40.

33. Tamada K, Ni J, Zhu G, et al. Cutting edge: selective impairment of CD8+ T cell function in mice lacking the TNF superfamily member LIGHT. J Immunol. 2002; 168(10):4832-5.

34. Liu J, Schmidt CS, Zhao F, et al. LIGHT-deficiency impairs CD8+ T cell expansion, but not effector function. Int Immunol. 2003; 15(7):861-70.

35. Mombaerts P, Iacomini J, Johnson RS, Herrup K, Tonegawa S, Papaioannou VE. RAG-1-deficient mice have no mature B and T lymphocytes. Cell. 1992; 68(5):869-77.

36. Chan V, Fong GC, Luk KD, et al. A genetic locus for adolescent idiopathic scoliosis linked to chromosome 19p13.3. Am J Hum Genet. 2002; 71(2):401-6.

37. Iida-Klein A, Zhou H, Lu SS, et al. Anabolic action of parathyroid hormone is skeletal site specific at the tissue and cellular levels in mice. J Bone Miner Res. 2002;17(5):808-16.

38. Wu J, Movérare-Skrtic S, Börjesson AE, et al. Enzalutamide Reduces the Bone Mass in the Axial But Not the Appendicular Skeleton in Male Mice. Endocrinology. 2016;157(2):969-77.

39. Yamada Y, Ando F, Niino N, Shimokata H. Association of polymorphisms of the osteoprotegerin gene with bone mineral density in Japanese women but not men. Mol Genet Metab. 2003; 80:344–349.

40. Langdahl BL, Carstens M, Stenkjaer L, Eriksen EF. Polymorphisms in the osteoprotegerin gene are associated with osteoporotic fractures. J Bone Miner Res. 2002; 17:1245–1255.

41. Kong YY, Yoshida H, Sarosi I, et al. OPGL is a key regulator of osteoclastogenesis, lymphocyte development and lymph-node organogenesis. Nature. 1999; 397(6717):315-23.

42. John V, Hock JM, Short LL, Glasebrook AL, Galvin RJ. A role for CD8+ T lymphocytes in osteoclast differentiation *in vitro*. Endocrinology. 1996; 137*:* 2457 – 2463.

43. Duhen T, Pasero C, Mallet F, Barbarat B, Olive D, Costello RT. LIGHT costimulates CD40 triggering and induces immunoglobulin secretion; a novel key partner in T cell-dependent B cell terminal differentiation. Eur J Immunol. 2004; 34(12):3534-41.

Figure 1. Skeletal morphology and bone structure of *Tnfsf14*^{-/-} mice. Representative images of alizarin red/alcian blue staining of bone and cartilage tissues of new born WT and *Tnfsf14*^{-/-} mice are shown (A). Also shown are representative whole-body microradiographs of 6-month WT and *Tnfsf14*^{-/-} mice after euthanasia (B). Mice were radiographed at 0-1-3-6 and 12 months of age, and measurements of the spine curvature were performed at different times and the quantitation reported in graph (C). Values are means ± SD; n = 4 (*Tnfsf14*^{-/-}), n = 3 (WT) per group. Representative hematoxylin-eosin stain of sagittal sections of decalcified vertebrae from 3- and 12 month WT and *Tnfsf14*^{-/-} mice together with calculated column height and number of cells for hypertrophic zone (HZ) and proliferative zone (PZ), respectively. Magnifications 10x (D). Von Kossa-stained vertebral sections from 3- and 6 month WT and *Tnfsf14*^{-/-} mice together with calculated cancellous bone parameters: bone volume/total volume (BV/TV), trabecular thickness (Tb.Th), trabecular number (Tb.N), and trabecular separation (Tb Sp) (E). Data are presented as mean ± SD. Statistics: t test. n = 5 mice per group. (Magnification: 2×) (E).
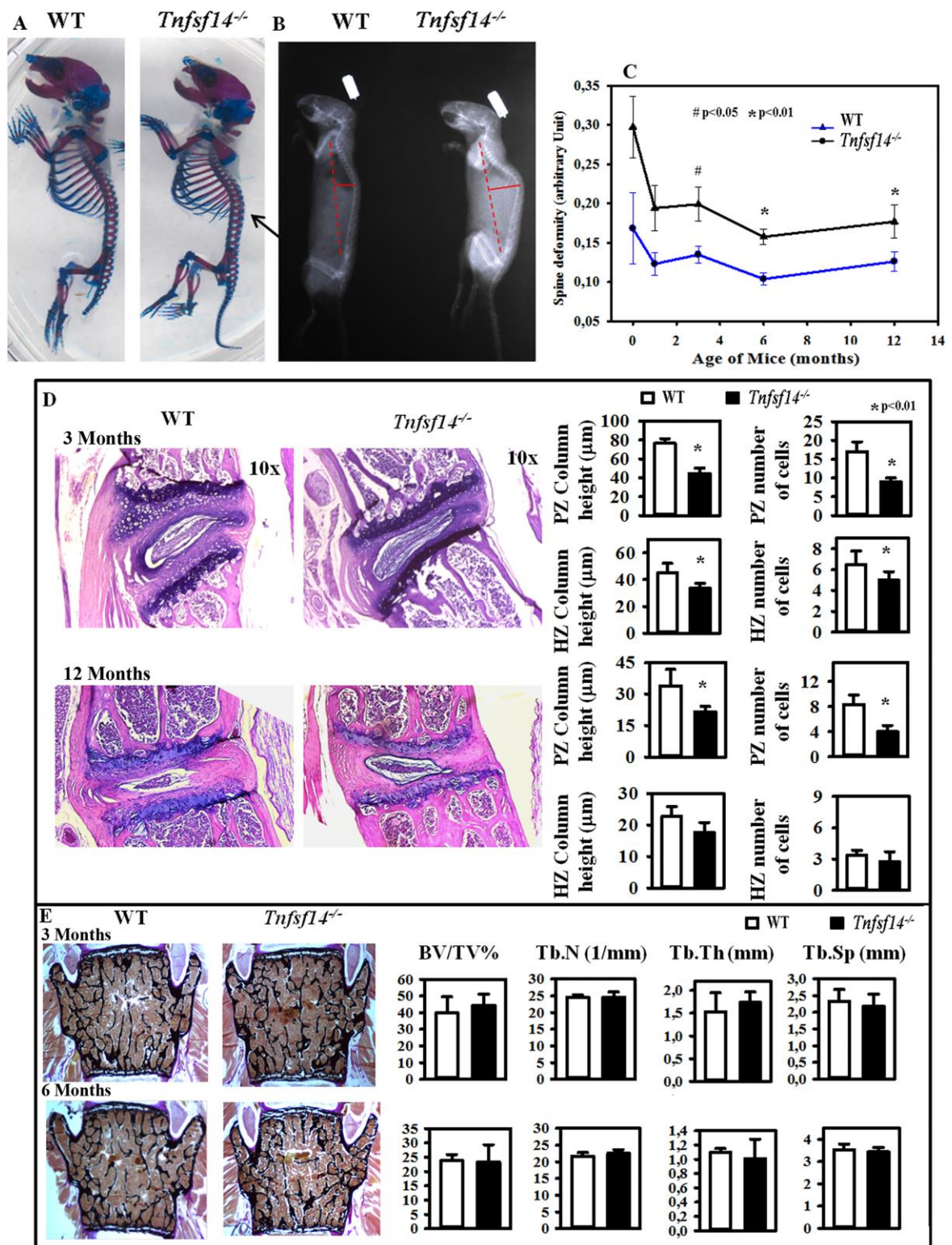
Figure 2. *Tnfsf14⁻/⁻* **mice showed decreased cancellous bone.** Representative micro-CT–generated section images of cancellous bone in femora harvested from 1-, 3-, 6- and 12-month old WT and *Tnfsf14⁻/⁻* mice. Graphs reporting calculated trabecular parameters at the metaphysis of WT and *Tnfsf14⁻/⁻* mice. Trabecular bone parameters included bone volume/total volume (BV/TV),

trabecular thickness (Tb.Th), trabecular number (Tb.N), and trabecular separation (Tb.Sp). Values are means ± SD. Statistics: Student's t test; n=6 for 1, 3, 12 month mice, n = 11 mice per group for 6 month mice. P values as shown.
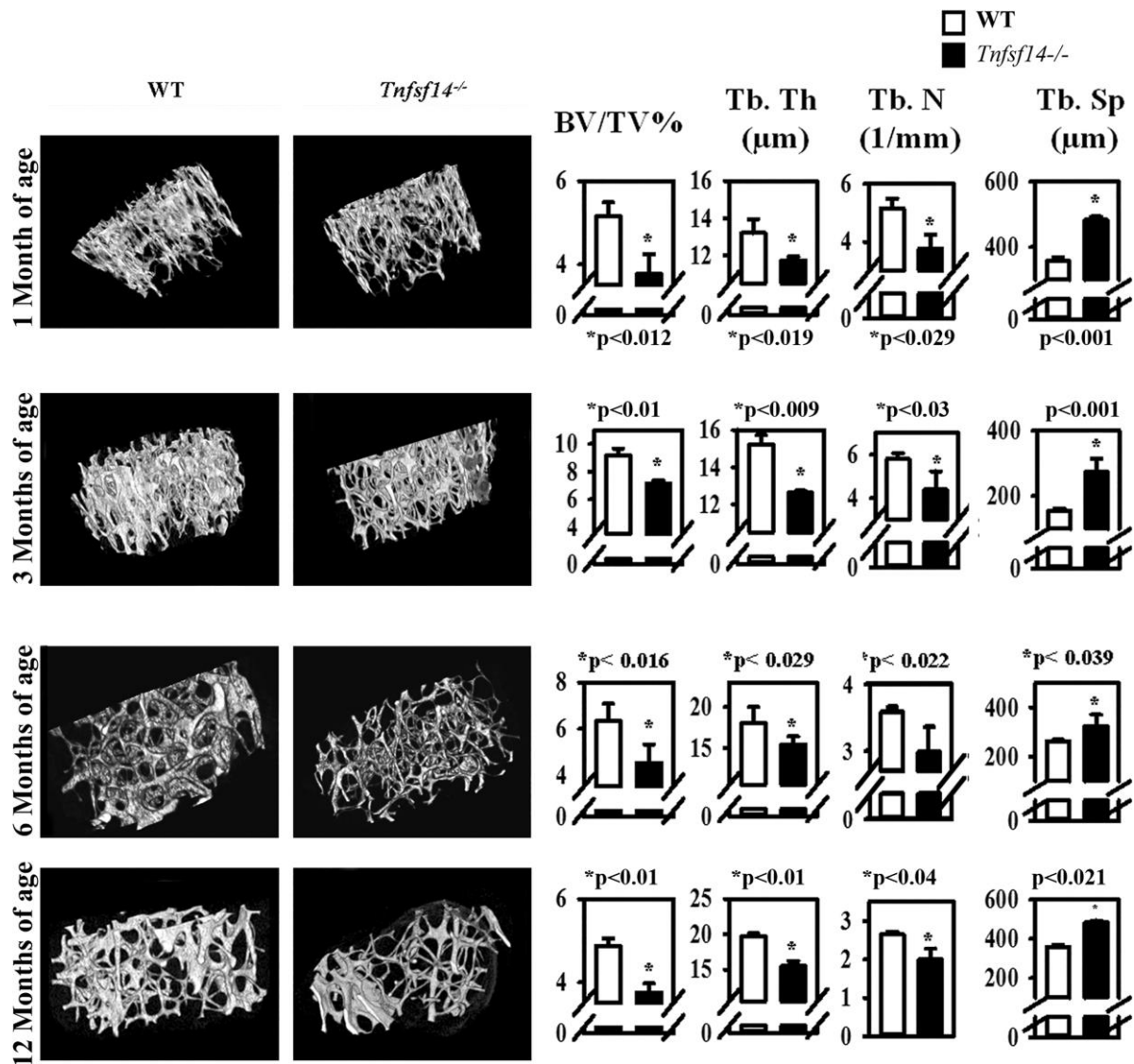
Figure 3. Altered bone cell activity in *Tnfsf14-/-* mice. Dynamic histomorphometry on cranial (A) and femoral (B, C) sections following timed injections (2 and 10 d before sacrifice) of xylenol orange and calcein, respectively. Cranial (A) and femoral (B,C) representative images are shown for 3 month WT and *Tnfsf14-/-* mice, together with calculated indices of bone formation, including mineralized mineral apposition rate (MAR), bone formation rate (BFR) and surface/total bone surface (MS/BS) (A). (Magnification: 20×). Also shown are representative images of toluidine blue-stained osteoblasts in femorus sections from 6 month WT and *Tnfsf14-/-* mice together with OB

number counts per bone perimeter (N.Ob/B.Pm), Magnification: 60× (D) and tartrate-resistant acid phosphatase-stained osteoclasts in femur sections from 6 month WT and *Tnfsf14⁻/⁻* mice, together with OC number per bone perimeter (N.Oc)/B.Pm, Magnification: 40×. (E). Data are presented as mean ± SD. Statistics: Student's t test, n =5 mice per group. P values as shown.
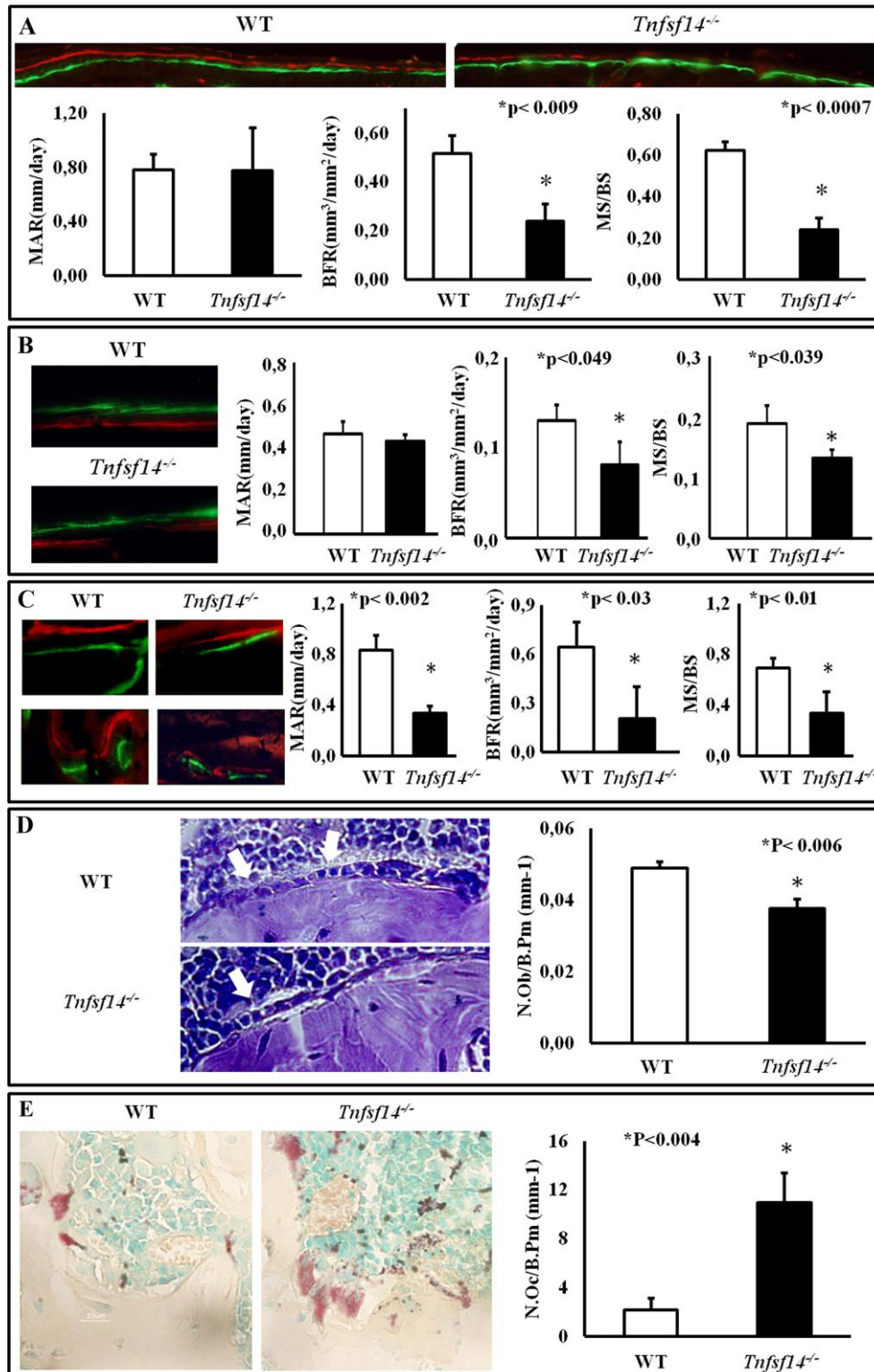
Figure 4. LIGHT regulates osteoclast formation and function in *ex-vivo* cultures.
Representative images are shown for tartrate-resistant acid phosphatase (TRAP)-stained cell cultures derived from 6-month WT and *Tnfsf14-/-* mice together with OC counts referred to 1-, 3-, 6- and 12- month mice. Magnifications 1x and 10x (A). Also shown are representative images of resorption area by mature osteoclasts from 6-month WT and *Tnfsf14-/-* mice plated on multiwell slides coated with a calcium phosphate film (von Kossa-stained) together with the calculation of the percentage (%) of resorption area referred to 1-, 3-, 6-, 12- month mice. Magnifications 1x and 10x (B). mRNA expression of differentiation genes, namely *Atpase6, Cathepsin K (Ctsk), Cfms, Dcstamp, Integrin β3 (Intβ3), Oscar, Rank, and Trap* are reported for mature OCs differentiated from the bone marrow of WT and *Tnfsf14-/-* mice (C).

Bone marrow stromal cells from 6-month WT and *Tnfsf14-/-* mice were grown in OB differentiation medium (50 μg/ml ascorbic acid and 10^{-2} M β-glycerophosphate). The percentage of alkaline phosphatase-positive CFU-F colonies (10 d) (D) and von Kossa-positive mineralized CFU-OB colonies (21 d) (E) from WT mice were calculated versus those from *Tnfsf14-/-* mice. Representative wells are shown (Magnification: 1×). Statistics by Student t test. n = 5 mice per group. P values as shown (WT vs *Tnfsf14-/-* mice).
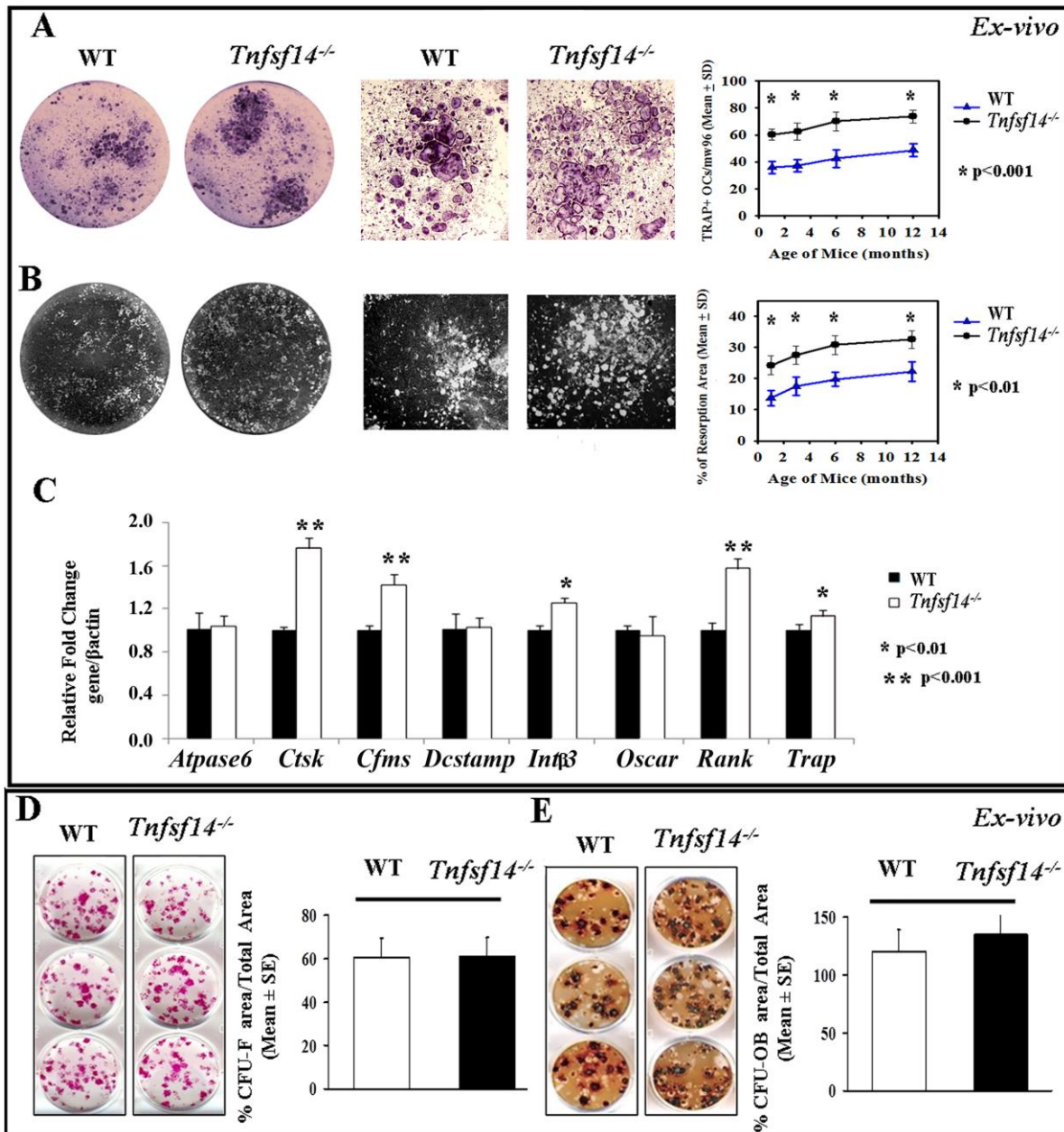
Figure 5. LIGHT effect on bone cell differentiation *in vitro*. (A) Representative images are shown for TRAP-stained osteoclasts derived from macrophage cultures of WT mice cultured in different conditions: MCSF (20 ng/ml) and RANKL (10 ng/ml), or MCSF (20 ng/ml) with 20 ng/ml aHVEM or 100 ng/ml aLTβR, ,or MCSF(20 ng/ml), RANKL (10 ng/ml) and 20 ng/ml aHVEM or 100 ng/ml aLTβR together cell counts in graph. (B) MC3T3 osteoblastic cell line were differentiated in the presence of ascorbic acid and β-glycerophosphate and the expression of *Ltβr* evaluated by real time PCR at 0 and 10 days of differentiation. Representative images are shown for ALP-stained osteoblasts derived from MC3T3 cultured without or with 100 ng/ml aLTβR in

osteogenic medium for 10 days. mRNA expression of differentiation genes, namely *Osterix (Osx),*
Runx2, Alkaline phosphatase (Alp), Atf4, Osteocalcin (Ocn), Dentin matrix acidic phosphoprotein 1
(Dmp1), Osteopontin (Opn), Collagen I (Cola1) are reported for MC3T3 cultured in osteogenic
medium and treated with 100ng/ml aLTβR for 2 and 10 days. (C) Mesenchymal cells from WT
mice were differentiated in the presence of ascorbic acid and β-glycerophosphate and the expression
of *Ltβr* evaluated by real time PCR at 0 and 10 days of differentiation. mRNA expression of
differentiation genes are reported for mesenchymal cells cultured in osteogenic medium and treated
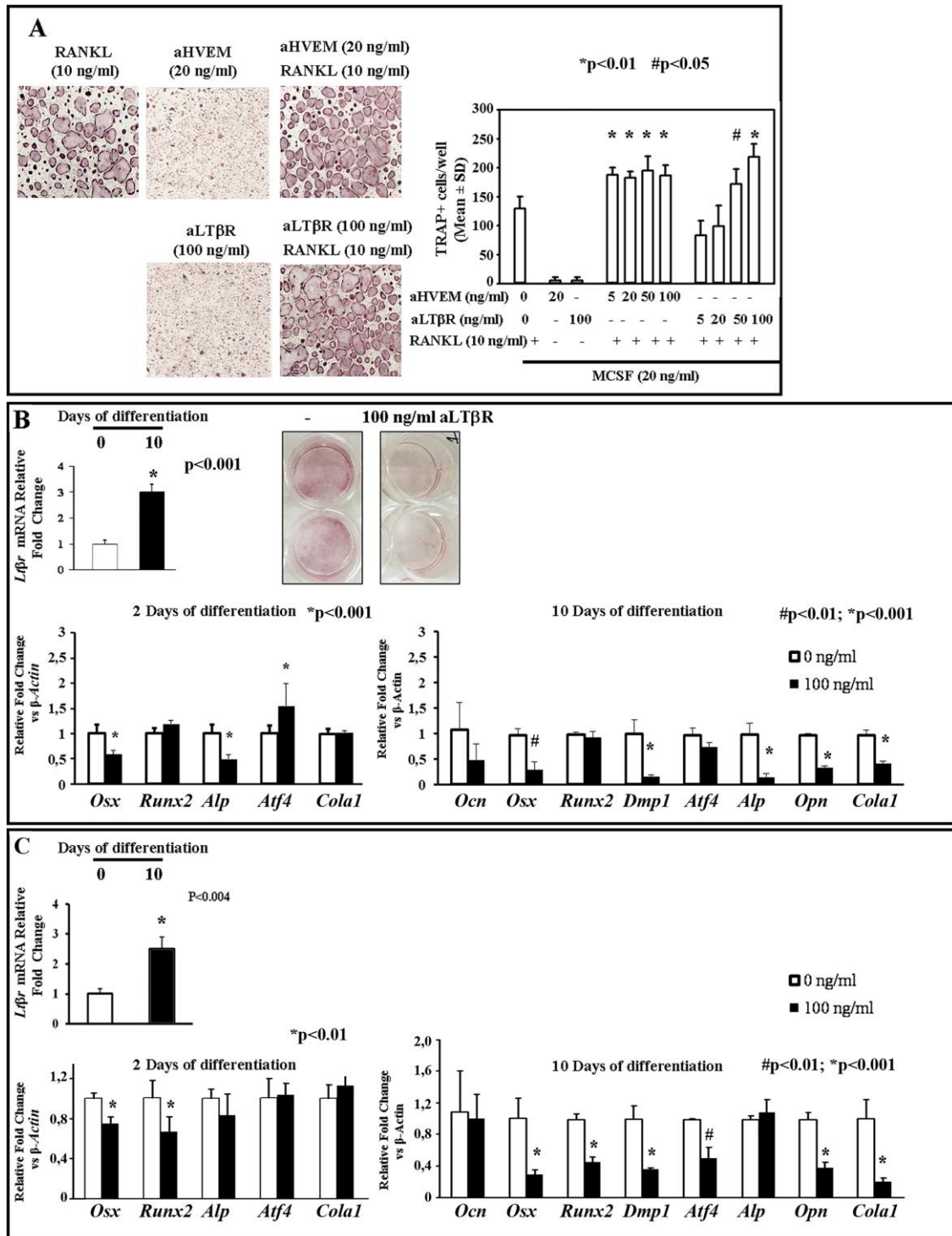with 100ng/ml aLTβR for 2 and 10 days. Statistics: t test, n=3. P values as shown.

Figure 6. (A) mRNA levels of *Rankl*, *Osteoprotegerin (Opg)* and *Rankl/Opg* ratio are reported for MC3T3 (seeded 15000/cm^2) cultured in osteogenic medium and treated with 100ng/ml aLTβR for 2 and 10 days. The media derived from the same cultures were assayed for the evaluation of RANKL and OPG levels as well as RANKL/OPG ratio by ELISA. **(B)** mRNA

expression of *Rankl* and *Opg* in osteoblasts and osteocytes isolated from WT and *Tnfsf14*^{-/-} mice. Statistics: t test, n=3. P values as shown.
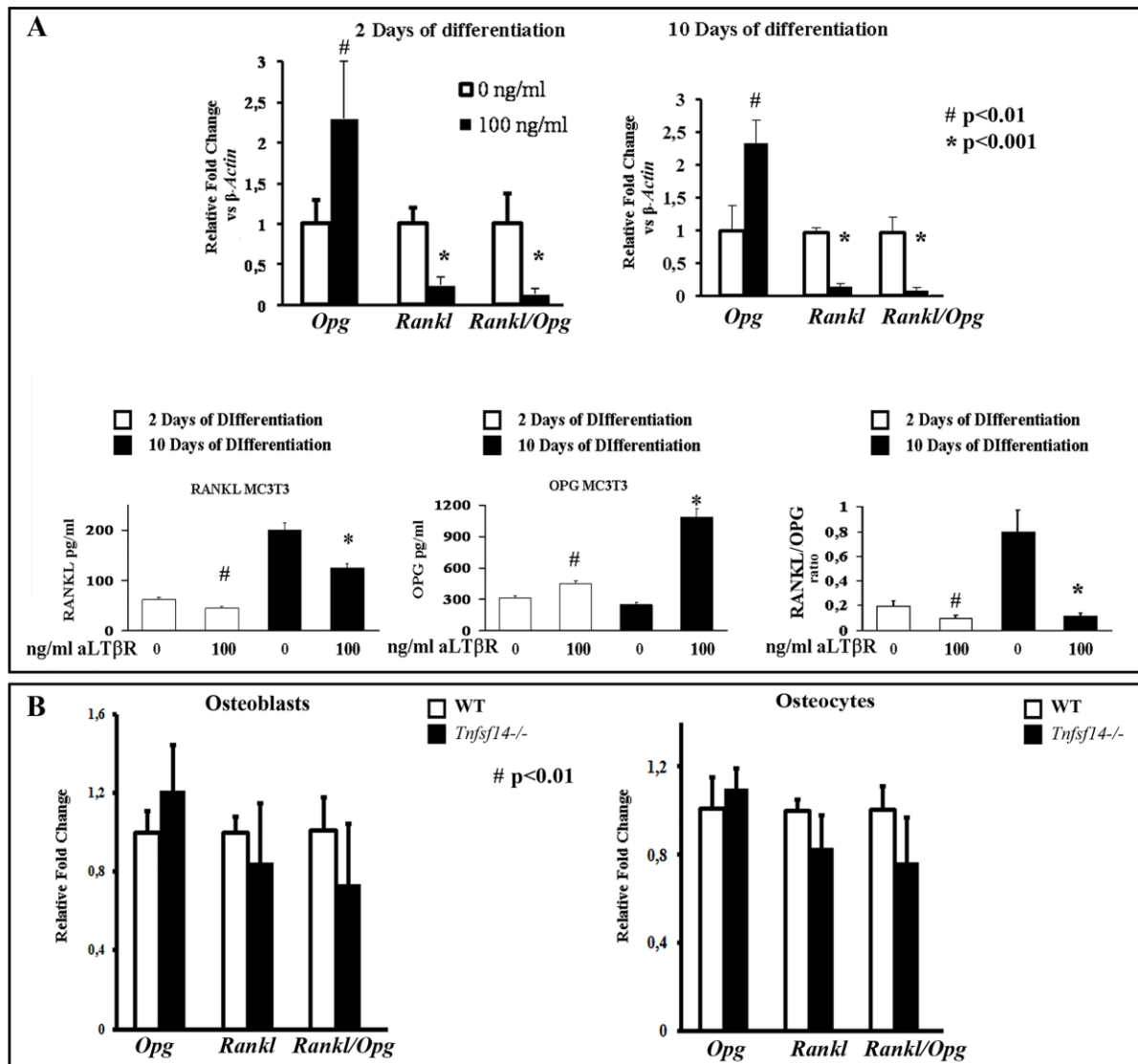
Figure 7. LIGHT affects OPG and Wnt10b expression. *Opg* (A), *Rankl* (B) and *Rankl/Opg* ratio (C) mRNA levels were determined in fresh lysates of total bone marrow (BM)-cells; OPG (D), RANKL (E) and RANKL/OPG ratio (F) levels were also measured by ELISA in media collected after 48 hours of cultures of total bone marrow cell from 1,3, 6, 12 month WT and *Tnfsf14*^{-/-} mice. *Opg* and *Rankl/Opg* ratio mRNA levels were also established in CD8+ T- (G), CD4+ T- (H), B220+IgM-IgD- (I), B220+IgM+IgD- (J), B220+IgM+IgD+ (K) and plasma cells (L) from the BM of 3 month WT and *Tnfsf14*^{-/-} mice. mRNA levels of *Opg* and *Rankl/Opg* ratio were determined in mRNA extracts of PBMCs (M), circulating CD8+ T- (N) and B-cells (O), as well as

spleen cells (P) from 3 month WT and *Tnfsf14*$^{-/-}$ mice. ELISA was used to detect OPG (Q), RANKL (R) and RANKL/OPG ratio (S) amounts in sera from 1, 3, 6, 12 month WT and *Tnfsf14*$^{-/-}$ mice. OPG levels were also measured in media derived from CD8+ T- and IgM+ cells treated with different concentration of aHVEM (0-100 ng/ml, T) or an IgG as control for 48 hours. CD8+ T-cells were isolated from 1, 3, 6, 12 month WT and *Tnfsf14*$^{-/-}$ mice and subjected to mRNA evaluation of *Wnt10b* expression (U). 100 ng/ml aHVEM or a control IgG were used to treat CD8+ T-cells and *Wnt10b* expression evaluated in CD8+ T-cells at mRNA level (V). *Wnt10b* mRNA levels were evaluated in osteoblasts isolated from WT and *Tnfsf14*$^{-/-}$ mice (W). Data are presented as mean ± SD. Statistics: Student's t test or ANOVA, n=5 mice per group. P values as shown.

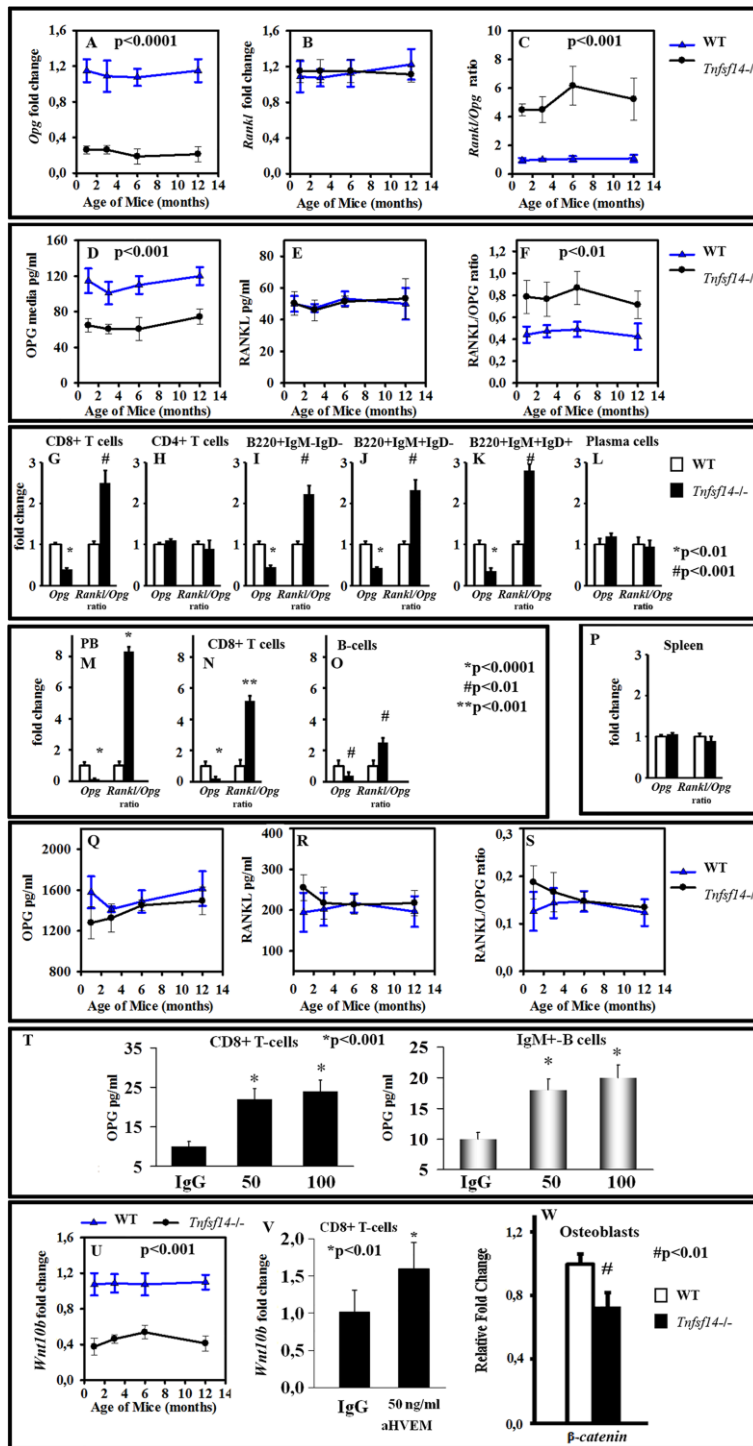**Figure 8.** *Rag⁻/Tnfsf14⁻* DKO **mice showed increased cancellous bone.** Representative micro-CT–generated section images of cancellous and cortical (A) bone in femora harvested from 3 month *Rag⁻/⁻* and DKO mice. Also shown are representative images of toluidine blue-stained osteoblasts in femorus sections from *Rag⁻/⁻* and DKO mice together with OB number counts per bone perimeter (N.Ob/B.Pm), Magnification: 60× (B) and tartrate-resistant acid phosphatase-stained osteoclasts in femur sections from WT and *Tnfsf14⁻/⁻* mice, together with OC number per

bone perimeter (N.Oc)/B.Pm, Magnification: 40× (C). mRNA levels of *Opg, Rankl* and *Rankl/Opg* ratio were determined in fresh lysates of total bone marrow (BM)-cells from *Tnsf14^{-}, Rag^{-/-}* and DKO mice (D). Statistics: Student's t test (A-C), ANOVA (D). n = 5 mice per group. P values as shown.
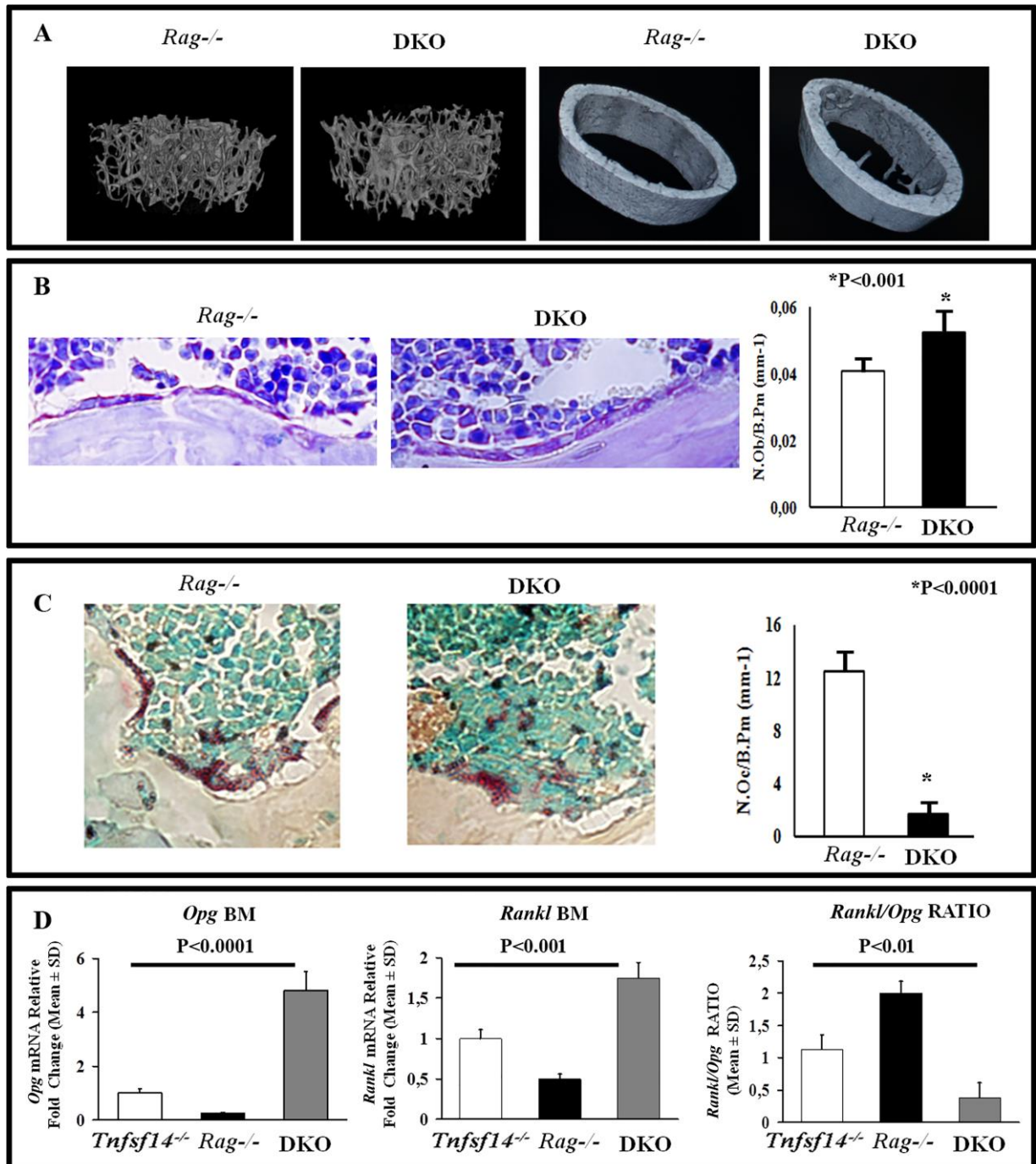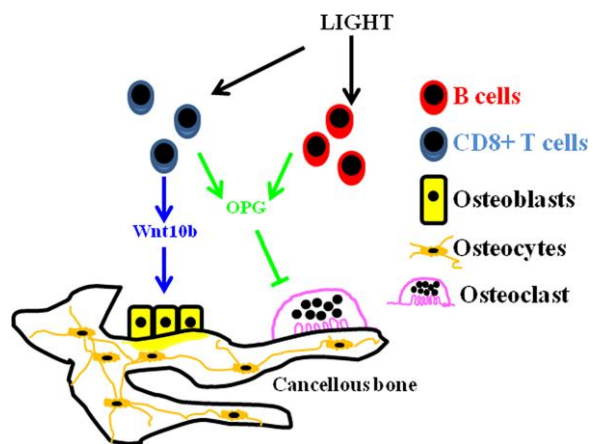

Figure 9. Model recapitulating the effect of LIGHT on cancellous bone.

LIGHT

B cells
CD8+ T cells
Osteoblasts
Osteocytes
Osteoclast

OPG

Wnt10b

Cancellous bone